pDART: Discrete algebraic reconstruction using a polychromatic forward model

Nathanaël Six, Jan De Beenhouwer and Jan Sijbers

***Abstract*—The discrete algebraic reconstruction technique (DART) is a tomographic method to reconstruct images from X-ray projections in which prior knowledge of the object materials' attenuation values is exploited. In monochromatic X-ray CT (e.g., synchrotron), DART has been shown to lead to high quality reconstructions, even with a low number of projections. However, most X-ray sources are polychromatic, leading to beam hardening effects, which significantly degrade the performance of DART. To reduce beam hardening artefacts, we developed an algorithm, pDART, that exploits sparsity in the attenuation values using DART and simultaneously accounts for the polychromaticity of the X-ray source. The results show that pDART leads to a vastly improved segmentation on simulated polychromatic data.**

***Index Terms*—Computed tomography, discrete tomography, DART, polychromaticity, beam hardening**

I. Introduction

COMPUTED tomography is a widely used technique for non-invasive imaging of a sample. Classical reconstruction techniques, e.g. Filtered Backprojection, assume a linear acquisition model and a large number of projections taken from a full angular view. When these requirements are not met, artefacts arise in the reconstruction.

One of the main sources of reconstruction artefacts is undersampling. When only few projections are available, the system of equations that needs to be solved for the reconstruction becomes severely underdetermined. By including prior knowledge about the sample, one can reduce this underdetermination, effectively decreasing the space of possible solutions. One of the ways this can be achieved is Discrete Tomography (DT), in which the grey levels in the image corresponding to the attenuation values of the object materials are assumed to be known a priori. This reduces the reconstruction from a continuous problem to a discrete problem. The *Discrete Algebraic Reconstruction Technique* or DART algorithm is one of the possible DT algorithms and has proven to be effective if the sample consists of few materials [1].

The DART algorithm relies on the same linearized acquisition model as most classical techniques; it assumes that the log-corrected normalized projection is the sum of attenuation values along a ray. This is an adequate model for a monoenergetic source, but not for a polyenergetic one. Due to this model mismatch, the reconstructed image will show beam hardening artefacts as the effective energy of the spectrum shifts upwards [2]. Beam hardening artefacts and the inability to clearly select a correct grey level for each material, lead to inaccurate reconstructions when DART is used in combination with polychromatic projections. One of the current methods for reducing beam hardening artefacts consists of placing metal filters in front of the source, to pre-harden the beam. However, the pre-hardened spectrum is still polychromatic and the filtering decreases the number of photons available for imaging.

We propose to combine the DART framework, with the *polychromatic Simultaneous Algebraic Reconstruction Technique* (pSART) introduced in [3], as the underlying reconstruction method. The pSART algorithm has previously successfully been combined with a Total Variation approach in [4]. This technique reconstructs a single grey level image, corresponding to a simulated monochromatic reconstruction, while using a polychromatic forward model.

In this paper, a short overview of DART and pSART is given, to clarify the models and algorithms that were used. Next, we explain the combined pDART algorithm and where it differs from the normal DART scheme. Finally, different discrete reconstructions from simulated polychromatic data are compared to demonstrate the improvements of the proposed method.

II. Method

A. Discrete reconstruction: DART

The DART algorithm is an efficient reconstruction method for discrete tomography. A complete discussion of DART can be found in [1]. We briefly recall the different steps in the DART algorithm:

1) **Initial reconstruction**: An algebraic reconstruction method (ARM) is performed to obtain an initial reconstruction $\boldsymbol{V}_0$.
2) **Segmentation**: Segment $\boldsymbol{V}_0$ based on the a priori knowledge of the grey levels and corresponding threshold values.
3) **Masking**: Choose a set of fixed and free pixels. The free pixels encompass all boundary pixels [1] and a small percentage of randomly chosen pixels.
4) **Reconstruction**: Perform a number of iterations of the ARM, on the set of free pixels only. The fixed

N. Six, J. De Beenhouwer and J. Sijbers are with Vision Lab, an imec research group at the University of Antwerp, Belgium (email: nathanael.six@uantwerpen.be)

[1] A pixel is called a *boundary pixel* if it has a neighbouring pixel with a different grey value.

pixels are kept at their segmented value. This gives us a reconstruction $\boldsymbol{V}$.

5) **Smoothing**: Apply smoothing to weaken the harsh fluctuations that can occur due to the segmentation.
6) **Iteration**: Set $\boldsymbol{V}_0 = \boldsymbol{V}$ and repeat steps 2-5 until a stopping criterion is met.

B. Polychromatic SART (pSART)

The pSART algorithm [3] is based on the same iterative scheme as SART [5]. In matrix form, the k^{th} update step can be expressed as:

$$\boldsymbol{V}^{(k+1)} = \boldsymbol{V}^{(k)} - \boldsymbol{C}\boldsymbol{A}^{\top}\boldsymbol{R}\left(\text{Proj}(\boldsymbol{V}^{(k)}) - \boldsymbol{s}\right), \qquad (1)$$

with $\boldsymbol{A}$ the system matrix of the acquisition geometry, $\boldsymbol{C}$ and $\boldsymbol{R}$ diagonal matrices with the inverse sums of the columns and rows of $\boldsymbol{A}$, respectively, Proj the forward projection operator, and $\boldsymbol{s}$ the sinogram. In the case of SART, $\text{Proj}(\boldsymbol{V}) = \boldsymbol{A}\boldsymbol{V}$. In pSART, however, a polychromatic forward projection is used instead.

The polychromatic projection P_{L_r} along the ray L_r[2] is modelled as:

$$P_{L_r} = \int_{\epsilon_{min}}^{\epsilon_{max}} I(\epsilon) \exp\left(-\int_{L_r} \mu(\boldsymbol{x}, \epsilon)\, \mathrm{d}\boldsymbol{x}\right) \mathrm{d}\epsilon, \qquad (2)$$

with μ the function giving the attenuation coefficient of the object at a point $\boldsymbol{x}$ and an energy level ϵ and I the X-ray source spectrum [2]. This model can be discretized over N_e total energy levels and N_m different materials to achieve the following form:

$$\hat{P}_{L_r} = \sum_{\epsilon=1}^{N_e} w(\epsilon) \exp\left(-\sum_{m=1}^{N_m} l_{r,m}\mu_m(\epsilon)\right). \qquad (3)$$

Here $w(\epsilon)$ is the weight for each energy level, $l_{r,m}$ the distance that ray L_r travels through material m, and $\mu_m(\epsilon)$ the attenuation coefficient of material m at energy ϵ. By log-correcting and normalizing the projection $\hat{P}_{L_r}$ from Eq. (3) we have:

$$\text{Proj}(\boldsymbol{V})_r = -\log\left(\frac{\hat{P}_{L_r}}{\sum_{\epsilon=1}^{N_e} w(\epsilon)}\right). \qquad (4)$$

The extra prior information needed for the pSART algorithm involves the spectrum: N_e and $w(\cdot)$ and the different materials in the sample: $\mu_m(\cdot)$ and N_m. Note that this knowledge about materials is also a prerequisite of the DART algorithm.

For the forward projection of $\boldsymbol{V}^{(k)}$, the line-lengths $l_{r,m}^{(k)}$ need to be calculated as follows. First, a reference energy ϵ_{ref} is chosen, which provides reference attenuation values $\mu_m = \mu_m(\epsilon_{ref})$. In each step, the reconstruction represents the monoenergetic attenuation map at energy level ϵ_{ref} [3]. Next, for each pixel v in the current reconstruction $\boldsymbol{V}^{(k)}$, with value $t_v \in [\mu_i, \mu_{i+1}]$, the fractions in the following decomposition are calculated:

$$t_v = \frac{\mu_{m+1} - t_v}{\mu_{m+1} - \mu_m}\mu_m + \frac{t_v - \mu_m}{\mu_{m+1} - \mu_m}\mu_{m+1}. \qquad (5)$$

[2] L_r is the ray from the source to the rth pixel on the detector.

These percentages are grouped, per material, in a mask $\boldsymbol{M}_m^{(k)}$. This essentially models each pixel v as the mixture of two materials. The $l_{r,m}^{(k)}$ are now found as the values in the product $\boldsymbol{A}\boldsymbol{M}_m^{(k)}$.

C. Polychromatic DART (pDART)

We propose a new algorithm based on the principles of DART and pSART that combines the benefits of both methods. As pSART returns a single grey value image, it is suited for combination with DART. However, due to the non-linearity of the polychromatic model and the assumptions made in the pSART model, changes to the masking step of DART and the material selection of pSART are needed.

Choosing pSART as the underlying reconstruction method implies that a weight vector and a matrix containing the energy dependent attenuation values and reference values have to be specified. This prior knowledge allows us to make a natural choice for the grey levels: the pSART algorithm already uses the reference values to decide which materials each pixel consists of and to reconstruct a single image which represents a monochromatic reconstruction at the reference energy level [3]. For this reason, the grey levels for segmentation are chosen to be the same as the reference attenuation values.

In the original DART approach, the forward projection of the fixed voxels is subtracted from the sinogram [1]. However,

$$\boldsymbol{s} - \text{Proj}(\boldsymbol{V}_{fixed}) \qquad (6)$$

as the new sinogram data to the pSART algorithm will not be equal to a reconstruction of the reduced system of equations. As a result, running the DART algorithm with the conventional settings will give rise to divergent behaviour. Because of the fundamental non-linearity of the polychromatic problem, the reconstruction on the reduced set of pixels cannot be performed in an analogue way to the monochromatic version. Instead, the line lengths through each material are calculated once in every DART iteration. The material locations are known, since the image is segmented. These same fixed numbers will be added to the calculated line lengths in each iteration of pSART. This way the pixel values are effectively fixed in the pSART iterations. However, the fixed values can no longer be grouped together in an updated sinogram.

To pass more information about the segmented interfaces to the pSART algorithm, a different interpolation is performed for boundary pixels. Instead of interpolating between the two closest reference values, interpolation is performed between the maximal and minimal attenuating material found within the neighbourhood of the boundary pixel.

For the implementation of the pDART algorithm, we implemented pSART in Matlab and used the DART framework from the ASTRA toolbox [6].

(a) Phantom image with three materials.

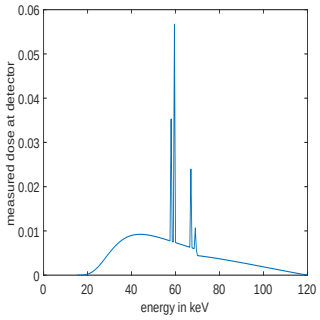

(b) Polychromatic spectrum of a 120keV source.

Figure 1: Phantom (a) and employed spectrum (b).

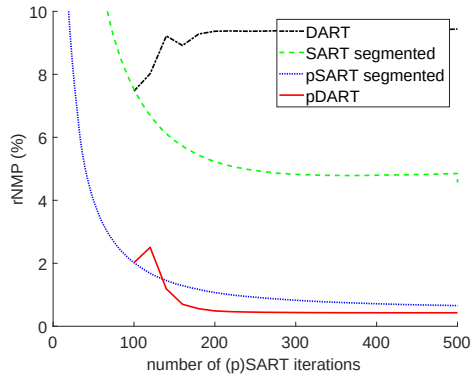

Figure 2: Plot of rNMP vs. (p)SART-iterations on 150 angles.

III. Experiments

To validate the proposed algorithm, simulation experiments were set up with an image quality phantom shown in Fig.1a. This phantom consists of three simulated materials on a vacuum background: water, cortical bone and titanium. The attenuation values at different energy levels were used from [7]. Different parallel beam polychromatic sinograms of the phantom were created, based on the weights and energy levels of a realistic spectrum, shown in Fig.1b. Sinograms were created with a variable number of angles, ranging from 2 to 500, equally spaced in the interval $[0, \pi)$. The forward model defined in Eq. (4) was used for the polychromatic projections. To limit inverse crime, the phantom was defined on a higher resolution grid than the reconstruction. To study the performance under noisy conditions, Poisson noise was added to the projections with 50 angles, based on different source intensities I_0, ranging from 5000 to 100000 photons per detector pixel.

From the simulated polychromatic sinograms, images were reconstructed with the following methods: FBP segmented with Otsu's method, pSART segmented, SART segmented, DART with manually optimized grey levels[3] and pDART. The segmentations of SART and pSART were performed with the same global threshold as DART and pDART, respectively.

All pDART reconstructions were performed with 1% random free pixels, 100 initial and 20 inner iterations of pSART. The same settings were used for DART. The percentage of free pixels was chosen as advised in [1]. When testing the influence of the variable number of angles, the error was measured after 300 (p)SART iterations, which corresponds to 10 (p)DART iterations.

For the noisy reconstructions we performed less (p)SART iterations per iteration of (p)DART: only 50 initial and 4 inner iterations, to prevent overfitting to noise. In this case, the error was measured after 210 (p)SART iterations. Due to the lower amount of initial and inner iterations, this corresponds to 40 (p)DART iterations. For the polychromatic reconstruction methods, the spectrum shown in Fig. 1b was rebinned to 18 bins. The reference energy level was set at 120keV, as higher energy levels lead to faster convergence [3].

All parameters (e.g. percentage of free pixels, number of inner iterations and reference energy level) were either chosen empirically or in accordance with the literature.

All reconstructions and projections were generated using the ASTRA toolbox [6].

[3]Out of the different available attenuation values, at the different energy levels, the one with the lowest reconstruction error was chosen.

IV. Results

To quantify the performance of pDART against segmented FBP, DART, segmented SART and segmented pSART, we computed the *relative number of mismatched pixels* or *rNMP* [1]. The effects of undersampling and beam hardening were very strong for FBP, so we have omitted FBP from all plots to improve visibility.

In Fig.2, the rNMP of the different methods is shown in function of the number of (p)SART iterations, for 150 projection angles between 0 and π. The rNMP for (p)SART was calculated at every iteration, whereas the rNMP for (p)DART was calculated at every DART iteration, i.e. every 20 (p)SART iterations. From Fig.2, one can observe that pDART converges more quickly than pSART. The original DART algorithm is outperformed by the other methods, except for FBP.

Next, the effect of varying amounts of projection angles on the rNMP was studied. These results are shown in Fig.3. Again, pDART outperforms the other methods in terms of mismatched pixels, reaching a lower stable rNMP and reaching this convergence point at a lower number of projections. This suggests that pDART benefits from both the beam hardening correction property of pSART and the imposed discreteness.

Lastly, the robustness to noise of the new method was studied. In Fig.4, the rNMP is plotted as a function of the beam intensity (represented by the photon count per detector element in the absence of attenuation). These simulations were performed for 50 projection angles.

Even in the presence of noise, pDART performs the best out of the different studied methods. However, comparing Fig. 4 with Fig. 3 shows that the influence of noise on our proposed method is still substantial.

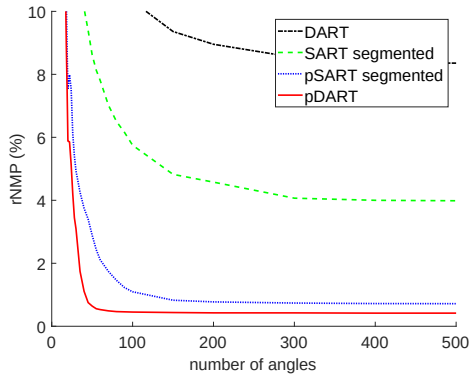

Figure 3: Plot of rNMP vs. number of angles, equally spaced in $[0, \pi)$.

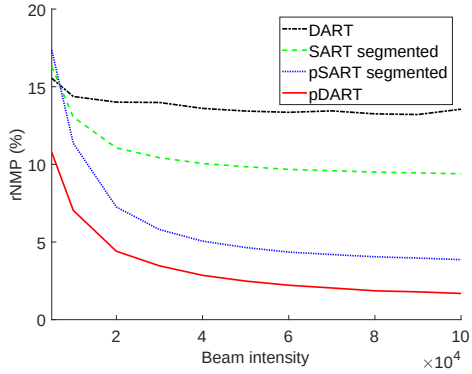

Figure 4: Plot of rNMP vs. different Poisson noise levels at 50 projection angles.

Finally, a comparison of the different reconstruction methods in the case of 50 noiseless projections can be found in Fig. 5. From this figure it can be observed that the two polychromatic methods show the least reconstruction artefacts, with the other methods showing beam hardening artefacts and streaks due to the low amount of projection angles. Both pSART and pDART have some mismatched black pixels in the interior, but the effect is less pronounced in the pDART reconstruction. Furthermore, it can be observed that pDART is the only algorithm, in our comparison, that accurately reconstructs the bar phantom in the center.

V. Conclusion

Many objects consist of a limited number of materials. This prior knowledge can be exploited in the reconstruction of images from X-ray projection data using discrete tomography. Current discrete tomography methods (such as DART), however, do not account for polychromaticity of X-ray sources, leading to various reconstruction artefacts. In this paper, pDART was proposed, a discrete tomography method that exploits sparseness in attenuation values, while taking a polychromatic projection model into account. Simulation experiments revealed that pDART results in substantially improved image reconstruction quality compared to DART or segmented versions of FBP, SART or pSART for polychromatic X-ray data.

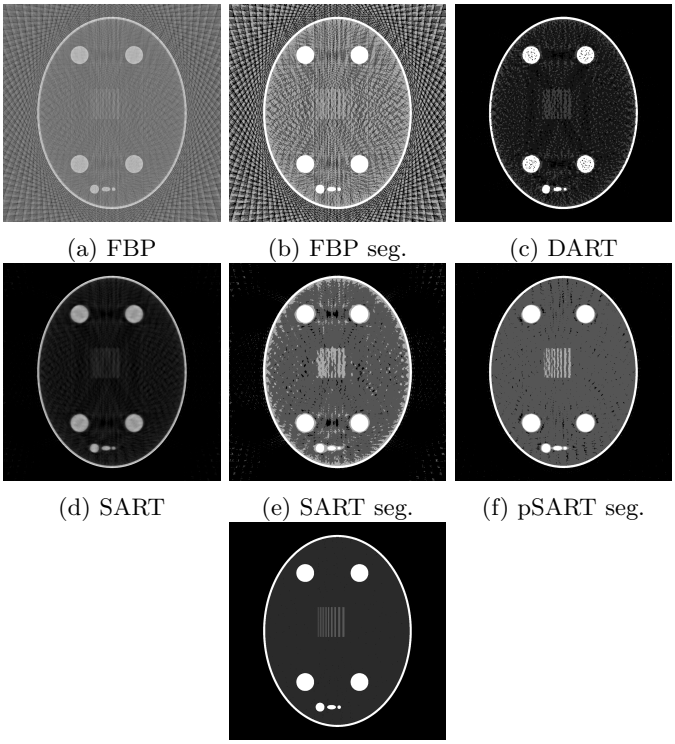

(a) FBP (b) FBP seg. (c) DART

(d) SART (e) SART seg. (f) pSART seg.

(g) pDART

Figure 5: Comparison of the different reconstruction techniques with 50 projection angles.

Acknowledgements

This research is funded by the FFG Bridge Early Stage project no. 851249: ADAM as well as the Fund for Scientific Research-Flanders (FWO, grant nr S004217N: MetroFlex). The authors would like to thank Arjan den Dekker for his insightful comments.

References

[1] K. J. Batenburg and J. Sijbers, "DART: a practical reconstruction algorithm for discrete tomography," *IEEE Transactions on Image Processing*, vol. 20, no. 9, pp. 2542–2553, 2011.

[2] T. M. Buzug, *Computed tomography: from photon statistics to modern cone-beam CT*. Springer Science & Business Media, 2008.

[3] Y. Lin and E. Samei, "An efficient polyenergetic SART (pSART) reconstruction algorithm for quantitative myocardial CT perfusion," *Medical Physics*, vol. 41, no. 2, 2014.

[4] T. Humphries, J. Winn, and A. Faridani, "Superiorized algorithm for reconstruction of CT images from sparse-view and limited-angle polyenergetic data," *Physics in Medicine & Biology*, vol. 62, no. 16, pp. 6762–6783, 2017.

[5] A. C. Kak and M. Slaney, *Principles of computerized tomographic imaging*. SIAM, 2001.

[6] W. van Aarle, W. J. Palenstijn, J. Cant, E. Janssens, F. Bleichrodt, A. Dabravolski, J. De Beenhouwer, K. J. Batenburg, and J. Sijbers, "Fast and flexible X-ray tomography using the ASTRA toolbox," *Optics Express*, vol. 24, no. 22, pp. 25 129–25 147, 2016.

[7] J. H. Hubbell and S. M. Seltzer, "Tables of X-ray mass attenuation coefficients," https://www.nist.gov/pml/x-ray-mass-attenuation-coefficients, National Inst. of Standards and Technology-PL, Gaithersburg, Tech. Rep., 1995.